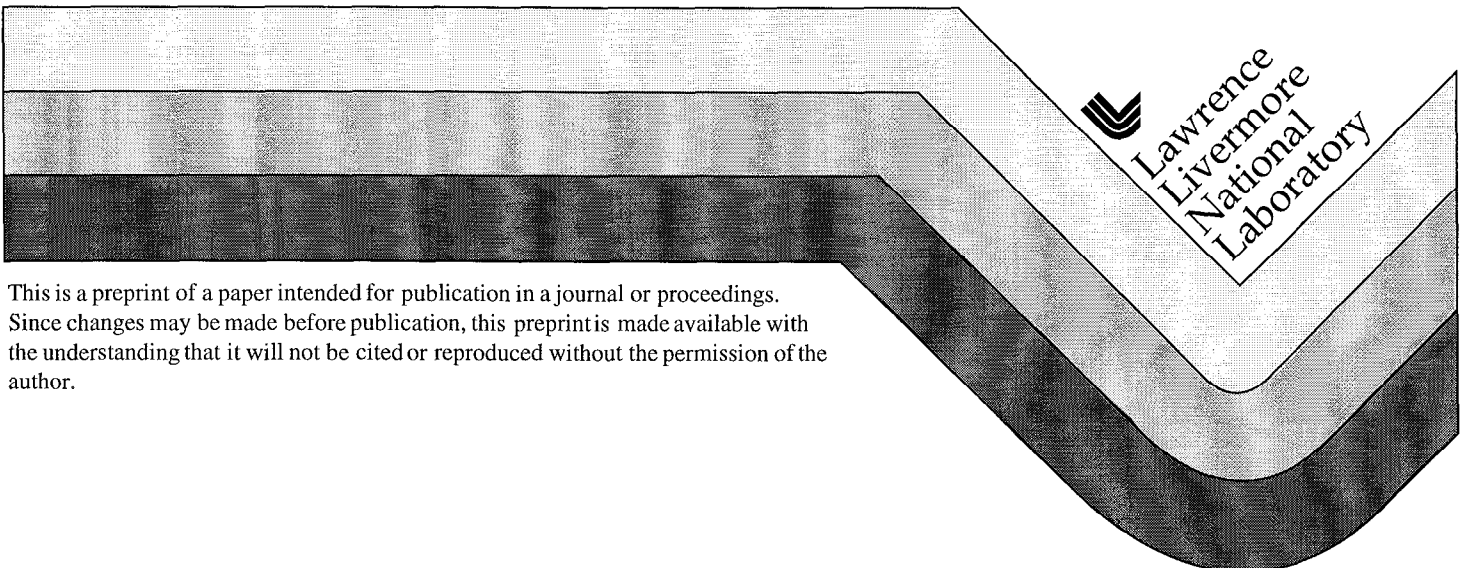# Emission Spectra and Particle Ejection During Visible-Laser Ablation of Graphite for Diamond-Like Coatings

Jim J. Chang
William McLean
Ernest P. Dragon
Bruce E. Warner
Lawrence Livermore National Laboratory

This paper was prepared for submittal to the
Photonics West '99 Symposium
San Jose, California
January 23-29, 1999

February 1999

DISCLAIMER

Emission spectra and particle ejection during visible-laser ablation of graphite for diamond-like coatings[*]

Jim J. Chang, William McLean, Ernest P. Dragon and Bruce E. Warner

Lawrence Livermore National Laboratory, P.O. Box 808, M/S L-463, Livermore, CA 94550

ABSTRACT

We have investigated the emission spectra of a carbon plume generated from graphite by a visible pulsed laser for diamond-like coatings (DLC). The laser utilized was a 300-watt class copper vapor laser with a pulse duration of ~40 ns. To better understand the laser-target interaction, we have visualized plume dynamics near the graphite surface via Schelieren method. We found that the laser ablation process was accompanied with explosive material ejection during pulsed laser deposition (PLD). The ejection of material started at about 500 ns after the onset of laser pulse and lasted for about 10 μs. The material ejection is very directional and introduced large amount of micro particulates in the DLC film. We have found that the use of a random phase plate to smooth the laser intensity profile effectively eliminated this ejection of material with additional advantage of higher coating rate. The spectra in the visible and UV of the plume emission were analyzed to correlate with DLC quality and coating rate. We have characterized the carbon plasma based on emissions from C, C_2, C^+ and C^{++} for laser peak intensities between 0.1 - 5 GW/cm^2. We have produced high-quality DLC with its coating rate optimized at laser peak power densities between 0.5 GW/cm^2 and 0.8 GW/cm^2. The kinetic energy of C^+ was estimated to be ~20 eV at this optimized coating condition. We found that greater C^+ kinetic energy at higher laser intensity does not necessarily produce better DLC. This process optimization enabled us to demonstrate a coating rate as high as 2000 μm-cm^2/hr. The C_2 swan-band emission from the plume was most pronounced in the optimized coating condition and was used as a process diagnostic tool.

Keyword: Pulsed laser deposition, laser ablation, diamond-like coatings, laser plasma.

1. INTRODUCTION

Thin film formation by pulsed laser deposition (PLD) has been routinely demonstrated at the laboratory scale for many elements and compounds. One of the distinct advantages of the PLD process is the near stoichiometric transfer from the ablation target to the desired substrate, a feature that is often difficult to achieve with conventional coating technologies such as magnetron sputtering or electron beam evaporation. However, PLD has only recently gained prominence in the deposition of diamond-like coatings (DLC) and high T_c superconductors[1-4]. DLC deposited by the vapor phase of carbon are amorphous and have many good properties [5]. They are hard coatings with low friction, transparent in the IR, electrically insulating, and chemically inert. Since the DLC are prepared without hydrogen using PLD, they have a higher density and index of refraction than the hydrogenated DLC obtained by plasma deposition processes.

In order for processes based on PLD to progress from bench top experiments to commercialization, a number of key issues must be resolved. The principle limitations of current PLD technology are low deposition rate (i.e., typically 10 μm-cm2/hr) [6,7], inclusion of micro particles in the film, and the difficulty in producing uniform coatings over large areas. In order to make the PLD for DLC more economically viable, we have investigated the laser-target interaction and the characteristics of the ablated carbon plume for process optimization. As a result, we have greatly improved the quality of our DLC with very low level of micro particle inclusions. A significant increase in coating rate has also been achieved in our laboratory, over 2000 μm-cm^2/hr. In this paper, we report the dynamics of laser ablation of graphite using a high-power pulsed visible laser. The measurements of laser-target interaction and plume emission spectra are also compared with the coating results.

---

2. EXPERIMENTAL APPARATUS

In this investigation, we used a 300-W class copper vapor laser in a master-oscillator-power-amplifier configuration[8]. The laser repetition frequency can be varied from below 1 Hz to greater than 5 kHz by adjusting the timing between the oscillator and the amplifier. Both of the copper laser green (511-nm) and yellow (578-nm) outputs were used for this work. The ratio of green/yellow in the output was typically 2:1. The pulse duration of the laser output was ~40 ns FWHM with a base-to-base pulse width of ~60 ns. The laser beam was focused to the graphite target by an achromatic lens located adjacent to a vacuum deposition chamber. The laser beam was aligned to the 1-inch-diameter graphite rod such that the ablated carbon plume is at 45 degrees from the incident beam, as illustrated in Fig. 1. The carbon plume generated by the laser moved toward directly to the sample port. The substrate to be coated was mounted within the sample port with a distance to the graphite surface of 7.6 cm. The laser peak intensity on the target could be varied from 0.1 GW/cm^2 to 5 GW/cm^2 by adjusting the laser power but maintaining a constant spot size. The vacuum chamber was typically kept a base pressure of 5×10^{-8} Torr. The pressure rose to ~10^{-6} Torr during PLD process.
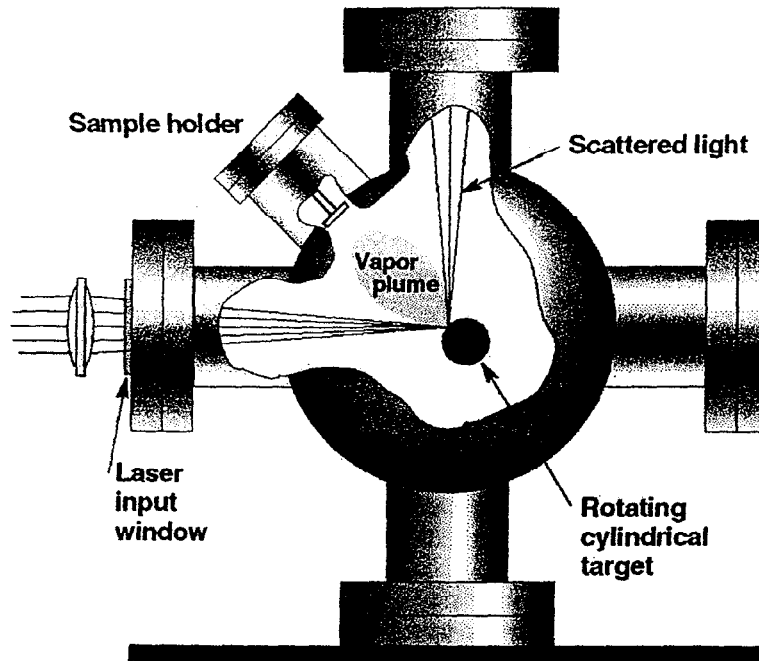

Fig. 1 The schematic of a PLD chambers; a high-purity graphite rod with 1" diameter is used as the target for producing DLC.

We used a 0.275-meter spectrometer with an optical multichannel analyzer (OMA) to measure the plume emissions. The OMA had a gated intensifier with 10-ns resolution to resolve the temporal development of the plume spectra. The schematic drawing of the setup is shown in Fig. 2a. The graphite rod rotated at approximately 1 RPS inside the deposition chamber. It could also be moved axially to keep a relatively fresh surface for laser ablation. The emission of the carbon plume was magnified and imaged to the entrance slit of the OMA. The plasma spectra were resolved spatially along the plume axis by moving the plume image relative to the entrance slit of the spectrometer. The width of the entrance slit was typically set at 10 μm for most of our measurements. The spectrometer was equipped with 300, 600 and 1200 l/mm gratings all blazed at 500-nm.

We used Schelieren technique to visualize the dynamics of carbon plume and material ejection during laser ablation. The schematic of the setup is illustrated in Fig. 2b. A frequency-doubled Q-switched Nd:YAG laser with an output of 10-ns green pulse (532nm) was collimated and used as a probe laser to illuminate the plume. The

YAG laser beam was spatial filtered to obtain a smooth and uniform beam profile. By adjusting the delay between the copper laser and the probe laser, we were able to visualize the dynamic of the laser-target interaction with 10-ns resolution. The knife-edge placed near the focus of the image lens was used to produce a Schelieren image. A 532-nm line filter was used to prevent both the plasma emission and the scattered copper laser light from entering the CCD camera.
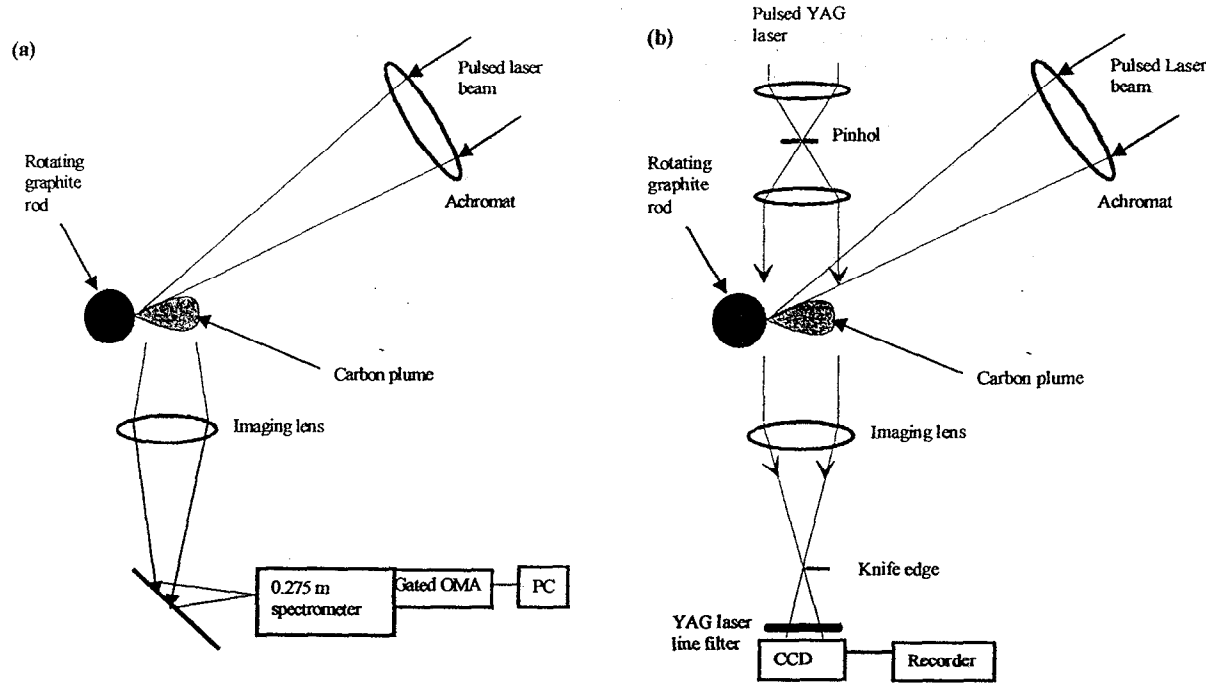

Fig. 2 (a) The setup for measuring emission spectra of the carbon plume. The graphite rod is placed in a vacuum deposition chamber. The plume is magnified and imaged into the entrance slit of the spectrometer. (b) The Schelieren setup for visualizing laser-target interaction using a 10-ns pulsed YAG laser.

2. CARBON PLUME AND EJECTION OF MICRO PARTICULATES

Figure 3 illustrates a sequence of Schelieren images near the target during laser ablation with various delays. These images were produced with a laser peak intensity of ~2 GW/cm^2 on the target. Note that a laser intensity of 1 GW/cm^2 is equivalent to 40 J/cm^2 in this work. The carbon-plume produced by the 40-ns laser pulse was only visible during the initial 200 ns by the Schelieren technique. However, noticeable material ejection from the target was found to start at ~500 ns after the onset of laser pulse. This explosive material ejection lasted for ~ 10 μs as illustrated in Fig. 3(c) & 3(d). Based on a sequence of Schelieren images, we estimate that the average speed of the ejected particles is approximately 400 m/sec. The temperature of the ejected material is estimated to be 2500 K – 3000 K based on their blackbody-radiation profile measured between 400 nm and 800 nm. It's worth noting that this explosive ejection of material was very directional as shown in Fig. 3(c) & 3(d). It is quite different from a melt splashing during laser machining of metals, which typically has a wide ejection angle[9]. The highly directional material ejection led to large amount of undesirable macro particulates in the DLC film. Singh has suggested that subsurface superheating induced micro explosion is the main cause of material ejection during laser ablation of superconducting material ($YBa_2Cu_3O_7$). The laser induced subsurface superheating, however, is not likely to occur on graphite because of its high absorption coefficient and high thermal conductivity[11]. Although the physical mechanism responsible for this material ejection is still not well understood, we found that it's a direct result of a non-uniform laser intensity profile (i.e., existence of a few hot spots) on the target.

Fig. 3   The Schlieren images of laser ablation (a) and material ejection (c & d) at different delays after the onset of laser pulse; (a) 50 ns, (b) 400 ns, (c) 1 μs, (d) 3 μs. The 40-ns laser pulse came from left.
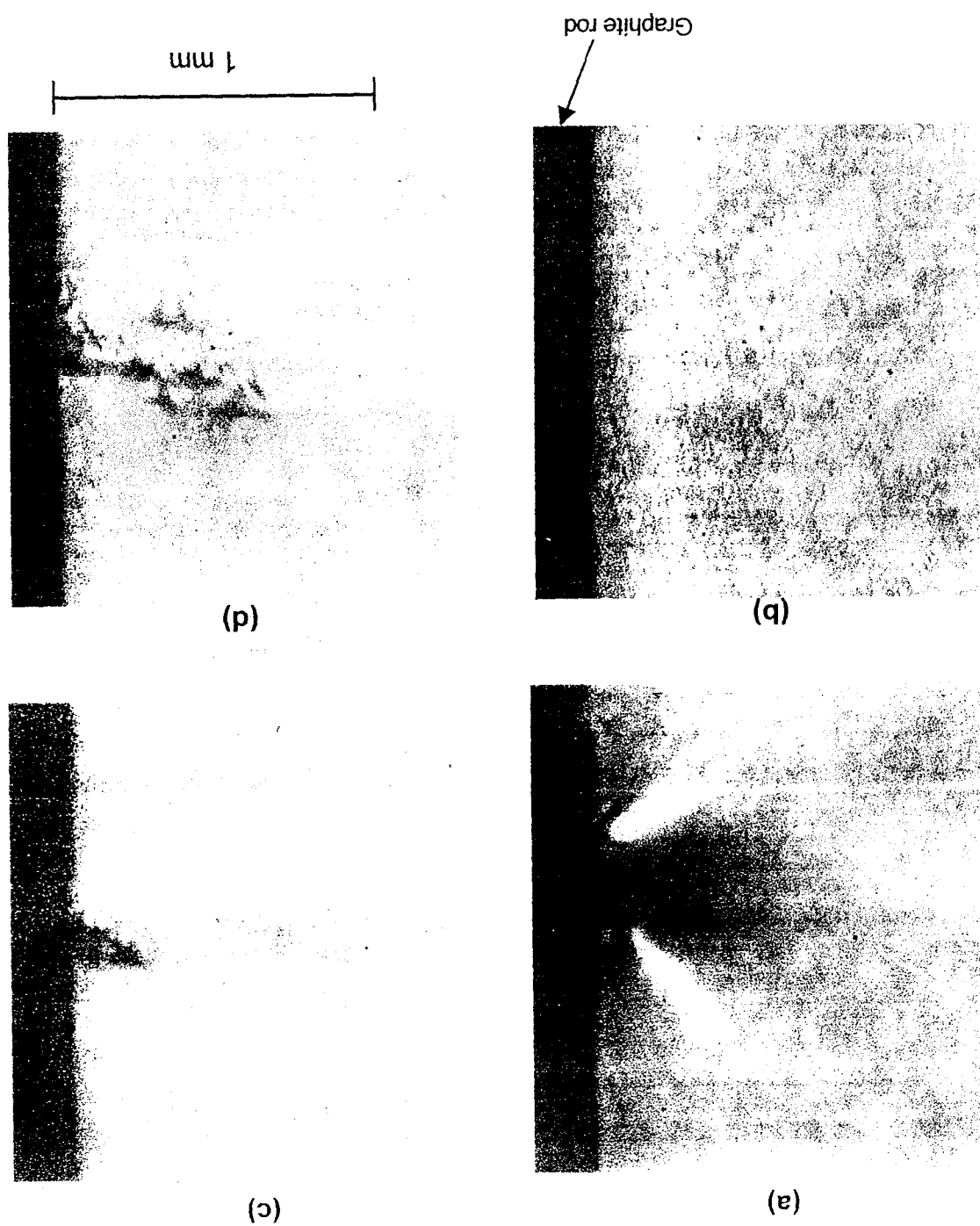
One of the methods to smooth the intensity profile of a laser focal spot is to use a random phase plate (RPP)[12]. A RPP has many phase-delay elements on its surface with specifically designed patterns to achieve a desired laser intensity profile. The phase-delay elements preferably to have a thickness of $n\lambda/2$ in order to create a phase π shift, where λ is the wavelength of the laser and n is the index of refraction of the phase-delay elements. A typical phase-plate pattern is illustrated in Fig. 4a where the delay elements are denoted by the darkened areas. This design is used in conjunction with a focusing lens to convert a circular laser beam to a focal point in the shape of an ellipse with a 400-micron major axis. The illuminated area becomes circular when this ellipse is projected onto a flat surface at an angle of incident of 45 degrees. The effect of inserting the RPP in front of a lens can be seen by examining the spatial intensity profile of the focus spot on the target, as illustrated in Fig. 4(b). With the addition of a RPP, the laser intensity profile on the target becomes gaussian-like with the elimination of hot spots that previously existed. The smoothing of the laser intensity profile using a RPP effectively eliminated any detectable material ejection from the graphite target, as examined by Schelieren images. As a result, the DLC produced with a RPP had significant fewer included particles. The resulting particle density is typically 2-8 particles within 40 μm by 40 μm areas with particle sizes of 50±10 nm wide and 200±50 nm height. This nanoparticle formation is believed mostly a result of condensation during the fast expansion of vapor plume[13]. The use of a RPP also
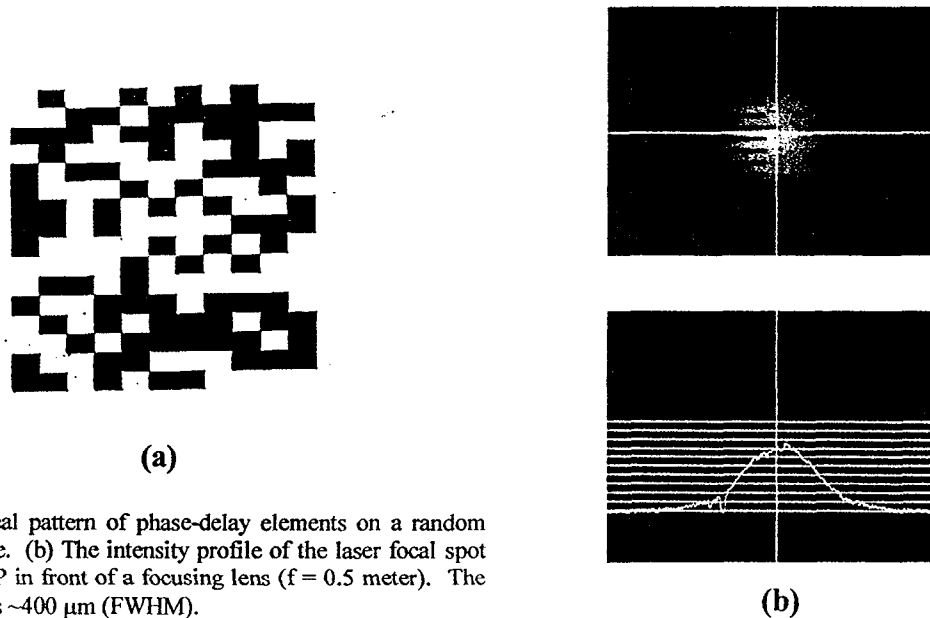

(a)

Fig. 4 (a) A typical pattern of phase-delay elements on a random phase plate. (b) The intensity profile of the laser focal spot with a RPP in front of a focusing lens (f = 0.5 meter). The spot size is ~400 μm (FWHM).

(b)

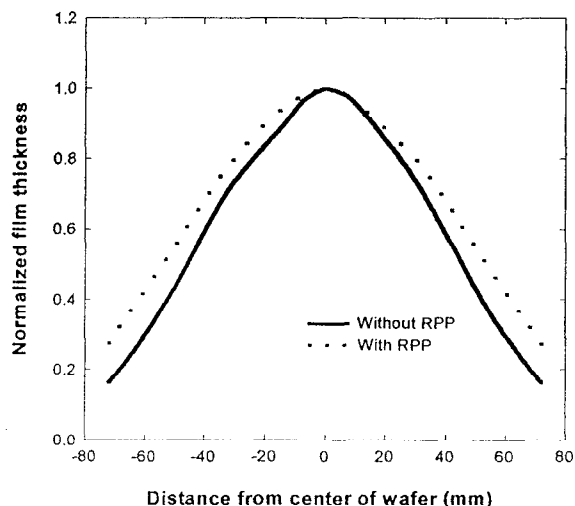

Distance from center of wafer (mm)

Fig. 5 The DLC deposition profiles on a silicon wafer with and without the use of a RPP .

increased the film deposition rate on a silicon substrate by as much as 50-60%. The spatial distribution of deposition thickness, as shown in Fig. 5, illustrates a more uniform film growth when use a RPP. The film deposition profile, which is typical represented by a cosin law in PLD, is improved from $\cos^{7.5}\theta$ to $\cos^{5.3}\theta$, where θ is the angle measured from the target surface normal. These improved features make PLD of DLC easier to scale up with greatly improved film quality.

3. EMISSION SPECTRA OF A CARBON PLUME

In this investigation, the spectra of the ablated carbon plume was measured mainly between 220 to 600 nm from direct emissions of C_2 dimer, C neutral, and C ions. The emission spectra were recorded at various time delays and downstream positions from the target. With a 1200 l/mm grating, we measured the C_2 Swan-band emission (d $^3\Pi_g$ $\Rightarrow$ a $^3\Pi_u$) near the target surface. The measured spectra illustrated in Fig. 6 shows the plume emission from 20 ns to 120 ns relative to the onset of the laser pulse. It is interesting to note that the initial broad band radiation is not necessarily greater at higher laser intensity, as shown in Fig. 6(a) and 6(c). The signal strength of the C_2 Swan band ($\Delta v = -1$), however, declines significantly as laser intensity increases from 0.8 GW/cm^2 to 4 GW/cm^2. We believe that the higher plasma temperature and electron density of the carbon plume at higher laser intensity lowers the possibility of C_2 formation (i.e., The C_2 dissociation energy is ~6 eV). The stronger C^+ and C^{++} emissions shown in Fig. 6(c) and 6(d) manifest a higher electron density and temperature. It's wrath noting that the line broadening of the C^+ emission at 0.8 GW/cm^2 is more pronounced than that at 4 GW/cm^2, especially later in time (i.e., 90 ns). This may be a result of slower plasma expansion at lower laser intensity. Figure 7 illustrates the plume emission in the UV range, which includes C, C^+, and C^{++} emissions at 247.8 nm, 251.2 nm, and 229.7 nm, respectively. The higher C^{++} emission resulting from higher plasma temperature at greater laser intensity is clearly shown in Fig 7 (c) and (d). The laser threshold for generating detectable ionic emission from ablation is found to be ~0.1 GW/cm^2.

The temporal development of C, C^+, and C^{++} emission illustrated in Figures 6 and 7 are plotted relative to the laser pulse, as shown in Fig. 8. It indicates that the ionic emission peaks near the end of laser pulse, when the carbon plume has the highest plasma temperature. The C and C_2 emissions, however, only start to appear at the end of
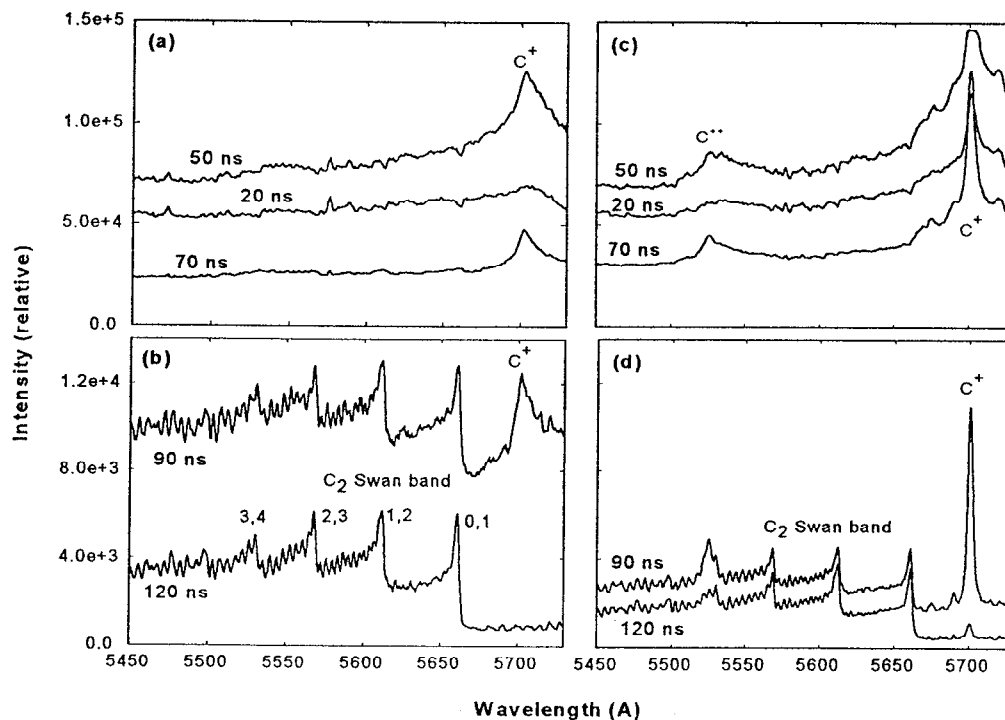

Fig. 6 Plume emission spectra near the target surface; the spectra were taken from 20 ns to 120 ns after the onset of laser pulse. The laser peak power was 0.8 GW/cm^2 (a & b) and 4 GW/cm^2 (c & d). Note that the vertical scales are the same between (a) & (c) and between (b) & (d).
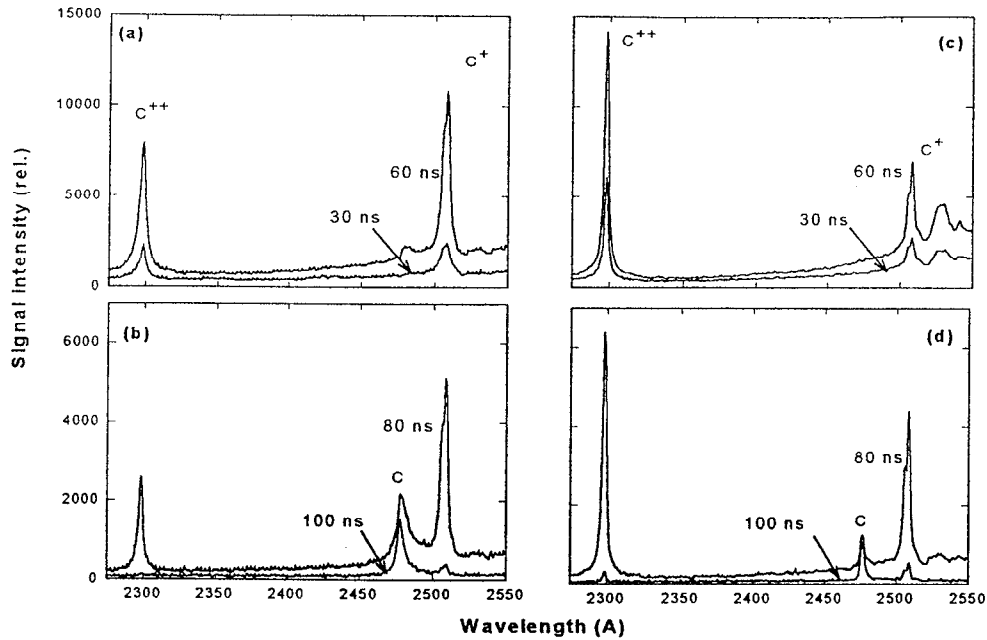
Fig. 7 Plume emission spectra near the target surface; the spectra were taken from 30 ns to 100 ns after the onset of laser pulse. The laser peak power was 0.8 GW/cm² (a & b) and 4 GW/cm² (c & d).
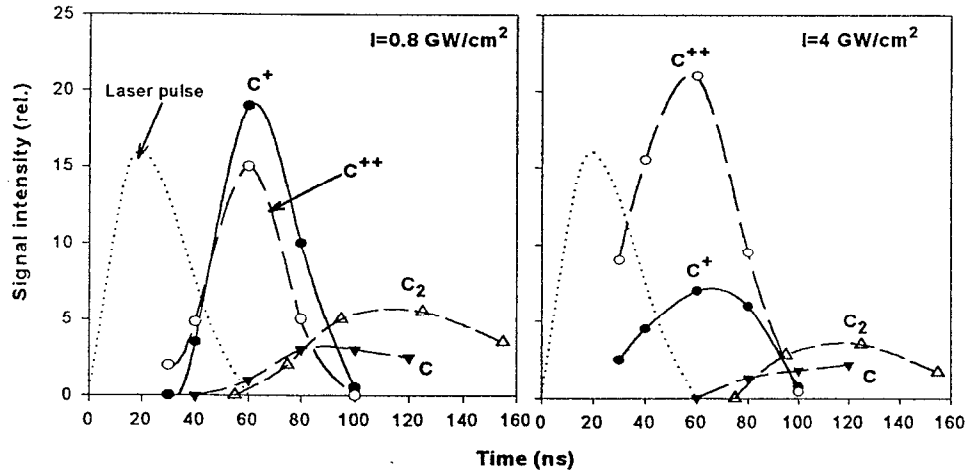

Fig. 8 The temporal development of carbon-plume emission near the graphite target at two laser peak intensities.

laser pulse. They reach their peaks at 100 -130 ns, when most of the ionic species have moved away from the target surface. Note that the C^{++}/C^{+} ratio increases significantly as the laser intensity increases from 0.8 GW/cm² to 4 GW/cm².

Figure 9 illustrates the spatial distribution of the emission along the plume axis at 100 ns. As illustrated in Fig 9a, the emission at a laser intensity of 0.5 GW/cm² is dominated by C and C_2 emission. We found that the Swan-band emission is strongest at this laser intensity. It's worth noting that the C_2 Swan band decays quickly (i.e., its radiative lifetime is ~110 ns) as it moves away from the target. The spectra of the carbon plume become mostly neutral and ionic emissions as the laser intensity increases to 2 GW/cm², as shown in Fig. 9(b). The temporally and spatially resolved emission measurement of the carbon plume enabled us to map the plume expansion after laser pulse. Figure 10 illustrates the spatial distribution of C, C^{+}, and C^{++} based on their emission at 247.8 nm, 426.7 nm, and 272.5 nm, respectively. Note that the 247.8-nm and 272.5-nm emission were detected by their 2'nd order as
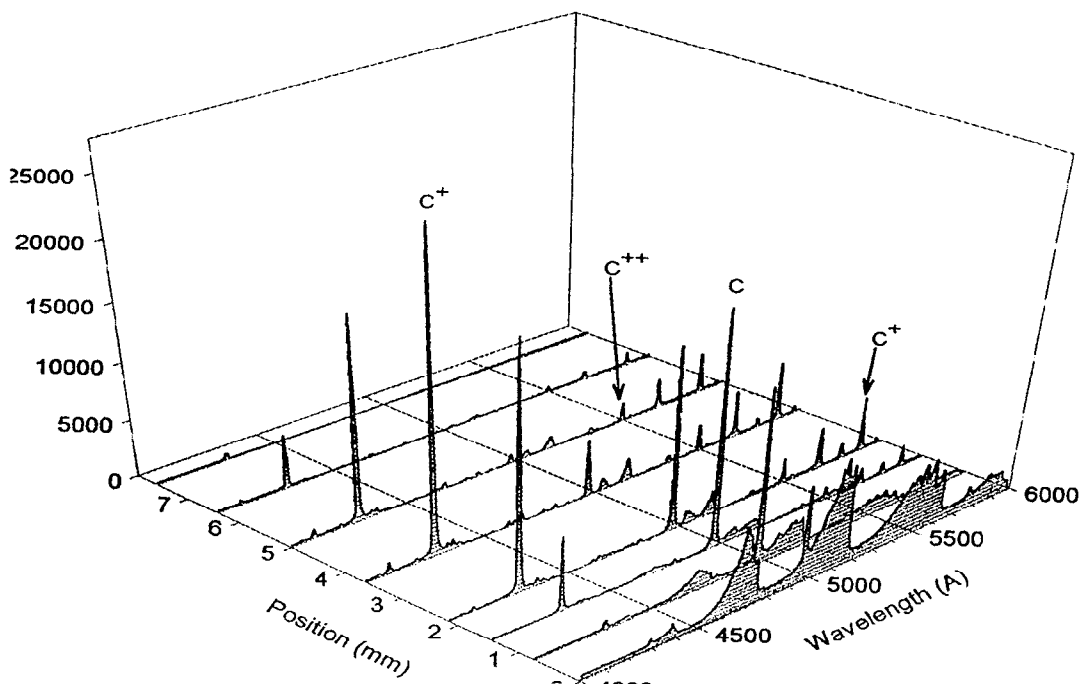
(a)
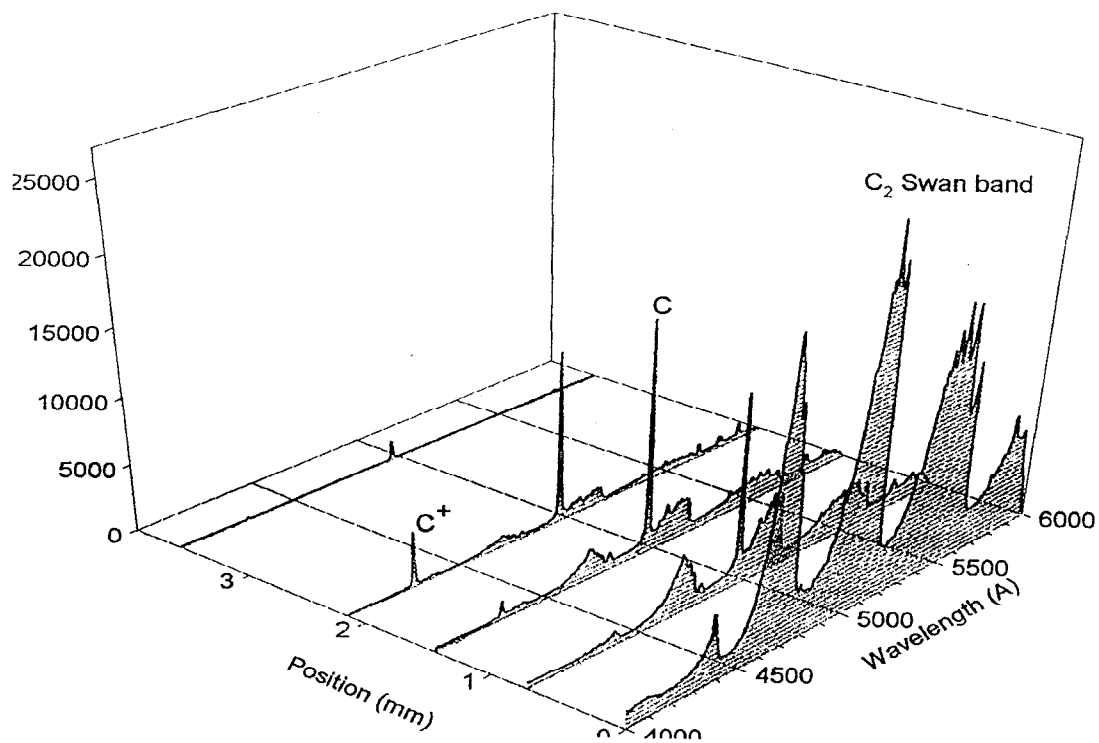
(b)

Fig. 9. The spatial distribution of plasma emission from laser ablated carbon plume; the spectra were taken at 100 ns after the onset of laser pulse with laser peak intensities of (a) 0.5 GW/cm^2 and (b) 2 GW/cm^2. The "Position" is the distance from the target.
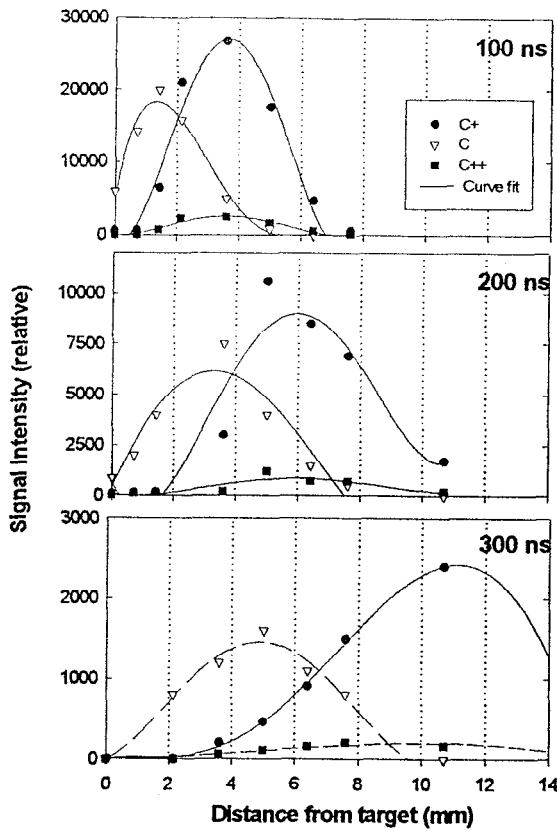
Fig. 10 The spatial distribution of plume emission from C, C^+, and C^{++} at 100 ns, 200ns, and 300 ns after the onset of laser pulse.
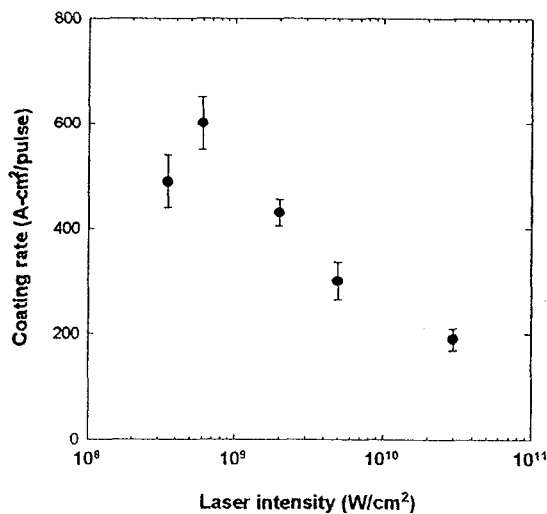

Fig. 11 The DLC coating rate vs. laser peak power on a silicon substrate.

shown in Fig. 9. The delay of the OMA was varied from 100 ns to 300 ns after the onset of the laser pulse. This figure clearly indicates that C^+ and C^{++} move jointly as a result of the Coulomb force in the ionized plume. The C neutrals lag behind the ionized particles with a slower speed. Based on this time-of-flight measurement, the kinetic energies of C neutral and C ions at a laser peak power of 2 GW/cm^2 are estimated to be 20 eV and 76 eV, respectively. The kinetic energies of C and C ions decrease to 15 eV and 20 eV, respectively, as the laser intensity is reduced to 0.5 GW/cm^2. It's worth noting that the ratio of C^{++}/C^+ remains about the same as the plume expands.

4. DEPOSITION RESULTS

The elimination of micro particulates using a random phase plate has enabled us to produce high quality DLC on polished Si (100) substrate. We have measured the coating rate of DLC at various laser intensities as plotted in Fig 11. It's found that the peak coating rate occurs at a laser peak intensity of 0.5-0.8 GW/cm^2. According to our measurements of plume emission, the variation of coating rate with laser intensity correlates to the intensity of the C_2 Swan-band emission. The reduction of coating rate at higher laser intensities is believed to be a result of plasma absorption. The plasma ignition threshold for carbon plume is similar to aluminum[14], which is measured to be ~2 GW/cm^2 [15]. No significant difference in DLC properties was measured at these laser intensities. The increase of ion kinetic energy form 20 eV to 76 eV as laser intensity increases from 0.5 – 2 GW/cm^2 has no noticeable effect on the coating quality.

Figure 12 shows Elastic Electron Loss Spectroscopy (EELS) spectra performed on the resultant material and on a graphite substrate. Typically there are three predominant features in an EELS DLC spectra. The elastic electron scattering peak is at the incident electron energy 500 eV. There is a peak ~6.6 eV below the incident energy which represents energy lost to the π-bonds of graphite (at 494 eV). The third feature is an unsolved broad plasma loss peak 30-40 eV below the incident energy. The lack of a π-π^* feature as compared to the graphite spectra indicates a DLC film[16]. With Atomic Force Microscopy (AFM) to measure surface roughness, we have determined a surface roughness of less than 10 nm with a 400-nm thick DLC. We have produced some films with RMS surface roughness as low as a few manometers.

6. CONCLUSION REMARKS

The PLD of DLC with visible laser light has been demonstrated with a 300-W copper laser running at 4.4 kHz. We have observed that explosive material ejection during laser ablation of graphite starts at ~500 ns after the onset of
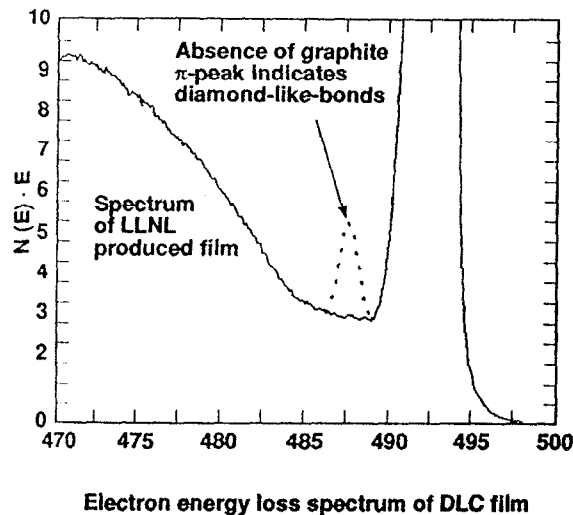
Electron energy loss spectrum of DLC film

Fig. 12. Electron energy loss spectrum of the DLC film produced with a copper laser.

laser pulse. The material ejection lasts for about 10 μs that leads to large amount of particle inclusion in the DLC film. Although the physical mechanism of this material ejection is still not well understood, we found that it's a result of non-uniform laser intensity profile on the target. With the use of a RPP to smooth the laser focal spot, we essentially eliminate the explosive material ejection. Additional advantages of using a RPP for PLD is a 50-60% increase of coating rate and a more uniform DLC film thickness.

It's found that the optimized coating rate for DCL is at a laser peak intensity of 0.5-0.8 GW/cm^2. Our investigation on plume emission spectra indicates that the coating rate correlates to the emission of C$_2$ Swan band. The kinetic energy of C$^+$ for the optimized coating rate is estimated to be ~20 eV based on a time-of-flight measurement. We found that higher kinetic energy of C$^+$ at higher laser intensities does not necessarily produce a better DLC quality. By optimizing the coating process base on our findings, we have demonstrated a coating rate of 2000 μm-cm^2/hr. This rate is ~100 times greater than any other known laser technology.

REFERENCES

1. J. Cuomo, D. Pappas, J. Bruley, and J. Doyle, J. Appl. Phys., **70**, p.1706, 1991.
2. D. Pappas, K. Saenger, J. Bruley, W. Krakow, J. Cuomo, T. GU, and R. Collins, J. Appl. Phys., **71**, p.5675, 1992.
3. F. Muller, K. Mann, and P. Simon, SPIE, **1858**, p.464, 1993.
4. F. Qian, R. Singh, S. Dutta, and P. Pronko, Appl. Phys. Lett., **67**, p.3120, 1995.
5. J. Angus and C. Hayman, Science, **241**, p.913, 1988.
6. B. Baren, J. Dubowski, and D. Norton, Mat. Res. Soc. Symp. Proc., **285**, p. 263, 1993.
7. B. Baren, J. Dubowski, and D. Norton, Mat. Res. Soc. Symp. Proc., **285**, p. 355, 1993.
8. J. Chang, Appl. Optics, **32**, p.5230, 1993.
9. B. Yilbas, J. Laser Application, **7**, p.147, 1995.
10. R. Sing, D. Bhattacharya, and J. Narayan, Appl. Phys. Lett., **57**, p.2022, 1990.
11. R. Sing, D. Bhattacharya, and J. Narayan, Appl. Phys. Lett., **62**, p.483, 1992.
12. S. Dixit, I. Thomas, B. Woods, A. Morgan, M. Henesian, P. Wegner, and H. Powell, Appl. Optics, 32, p.2543, 1993.
13. D. Geohegan, A. Puretzky, G. Duscer, and S. Pennycook, Appl. Phys. Lett., **72**, p.371, 1998.
14. M. Shannon and X. Mao, paper presented at the OSA Annual Meeting, Portland, Oregon, 1995.
15. J. Chang, and B. Warner, Appl. Phys. Lett., **69**, p.473, 1996.
16. P. Murry and D. Peeler, J. Elec. Mater., **23**, p.855, 1994.